Acta Crystallographica Section D
Biological Crystallography
ISSN 0907-4449

Structural and biochemical analyses reveal a monomeric state of the bacterial lipocalin Blc

André Schiefner, Lorenz Chatwell, Daniel A. Breustedt‡ and Arne Skerra*

Munich Center for Integrated Protein Science (CIPS-M) and Lehrstuhl für Biologische Chemie, Technische Universität München, Freising-Weihenstephan, Germany

‡ Present address: F. Hoffmann-La Roche Ltd, 4070 Basel, Switzerland.

Correspondence e-mail: skerra@tum.de

Received 10 July 2010
Accepted 1 October 2010

PDB Reference: monomeric Blc, 3mbt.

The first bacterial member of the lipocalin protein family, Blc, was identified in *Escherichia coli* as an outer membrane lipoprotein that is expressed under conditions of environmental stress. Previous crystallographic studies in space group $P2_12_12_1$ with two molecules per asymmetric unit, supported by static light-scattering experiments in solution, indicated that Blc may form a functional homodimer with lysophospholipid binding activity. Here, a new crystal structure of recombinant Blc in space group $I4_122$ with one molecule in the asymmetric unit is described. The crystal packing differs considerably from that observed previously, which was determined using an N-terminally extended version of Blc dubbed 'Blc-X'. In particular, the characteristic large interface region that was previously described as being responsible for stable dimer formation is absent in the $I4_122$ crystal structure. Thus, the dimerization behaviour of Blc-X was most likely to be caused by the additional N-terminal peptide segment resulting from the cloning strategy employed. In contrast, we used a native-like N-terminus for Blc with just the lipid-anchored first Cys residue replaced by Ala. The fully monomeric status of this recombinant version of Blc in solution was confirmed by size-exclusion chromatography as well as analytical ultracentrifugation. Consequently, these data shed new light on the previously postulated lipid-binding mechanism and biological role of Blc. Beyond this, our findings illustrate that cloning artefacts, which frequently result from recombinant protein production for structural studies, must be considered with special caution when interpreting oligomerization and/or conformational effects.

1. Introduction

The lipocalins represent a family of functionally diverse small proteins comprising 160–180 residues that share high conservation at the tertiary structural level while having weak amino-acid sequence homology (Flower *et al.*, 2000; Skerra, 2000). Their fold is dominated by an eight-stranded antiparallel β-barrel with an α-helix attached to its side, in which four structurally variable loops, which connect neighbouring β-strands at the open end of the barrel, form the entrance to a ligand pocket. Further hallmarks are three structurally conserved regions (SCRs; Flower, 1996), which assist the identification of new lipocalins at the primary structure level.

Lipocalins were initially described in eukaryotes and have only more recently been identified in Gram-negative bacteria (Flower, 1996; Bishop *et al.*, 1995; Bishop, 2000). However, it seems that the lipocalins may in fact have originated in Gram-

negative bacteria and were later horizontally transferred from the endosymbiotic α-proteobacterial ancestor of the mitochondrion to the eukaryotic genome. Bacterial lipocalin (Blc) was first discovered in *Escherichia coli* (Bishop *et al.*, 1995), but sequence analyses have indicated the existence of at least 20 other bacterial lipocalins, for example in *Citrobacter freundii*, *Vibrio cholerae* and many other Enterobacteriaceae.

Blc belongs to the class I outer membrane lipoproteins, which carry a type II signal peptide at the N-terminus that directs export into the bacterial periplasm. After signal peptide processing, the protein becomes anchored into the inner leaflet of the outer membrane (Bishop *et al.*, 1995) *via* an intensely lipid-modified amino-terminal cysteine residue. The *blc* promoter is mainly induced at the onset of the stationary growth phase *via* the *rpoS* σ factor, which generally directs gene expression for adaptation to starvation and high osmolarity or other conditions known to exert stress on the cell envelope. The *blc* gene is poorly transcribed, suggesting that the normal concentration of Blc in the outer membrane is low.

Other findings imply the involvement of Blc in bacterial host pathogenesis (Bishop, 2000). The *blc* genes of some Enterobacteriaceae are physically linked to the *ampC* gene, which encodes a serine β-lactamase on the chromosome but also appears to be genetically recombined into different plasmids. This co-localization suggests that the *blc* gene may be involved in antibiotic resistance. Furthermore, bacterial lipocalins play a role in the host immune response as many components of the bacterial cell envelope provide so-called pathogen-associated molecular patterns for surveillance. One relevant component is the *N*-acyl-*S*-*sn*-1,2-diacylglyceryl-cysteine modification at the N-terminus of the bacterial lipoproteins, which permits macrophages and other immune cells to recognize Blc *via* CD14 and the Toll-like receptor 2.

The first crystal structure of an N-terminally extended version of Blc, called Blc-X (Campanacci *et al.*, 2004), revealed the β-barrel fold characteristic of the lipocalin family and was followed by a second crystal structure of Blc-X in complex with the fatty acid vaccenic acid (Campanacci *et al.*, 2006). Both structures belong to space group $P2_12_12_1$, with isomorphous unit-cell parameters and an overall r.m.s. deviation of 0.1 Å for 167 C^{α} atoms. Based on the identification of a buried surface of 786 and 825 Å^2, respectively, for the two distinct Blc-X molecules *A* and *B* within the asymmetric unit and also on static light-scattering measurements in solution, a functional Blc dimer was proposed. Notably, the fatty-acid ligand was bound in the cavity of just one molecule of the dimer and was involved in only a few additional contacts to the other molecule, which was explained by an asymmetric interaction of the two Blc-X monomers. However, the binding of vaccenic acid did not lead to detectable conformational changes within the Blc-X dimer (Campanacci *et al.*, 2006).

Factors that influence the quaternary structure of proteins are of particular interest because ligand specificity and affinity often depend on oligomerization, thus changing the biological activity. Unexpectedly, when we studied the biochemistry and structure of recombinant Blc overproduced with a different *E. coli* expression vector we found striking evidence that Blc behaves as a stable monomer in solution. This observation was backed by its crystallization in a different space group, thus necessitating critical reassessment of its previously proposed oligomeric structure and physiological role.

2. Materials and methods

2.1. Vector construction

The coding sequence for Blc was amplified from genomic DNA of *E. coli* K-12 strain TG1/F$^-$ (Kim *et al.*, 2009) *via* PCR according to a published procedure (Skerra, 1992) using phosphorothioate primers 5′-CCG CCA GTT CTC CTA CGC CGC CG-3′ (which also introduced the Cys1-to-Ala mutation) and 5′-GCT ACC AGG CTG CTG TAC CC-3′. The unique amplification product was purified by agarose gel electrophoresis, phosphorylated with T4 polynucleotide kinase (New England Biolabs, Beverly, Massachusetts, USA) and ligated with the expression vector pASK75-strepII (Skerra, 1994; Schmidt & Skerra, 2007), which had been cut with *Stu*I and *Eco*47III and dephosphorylated using shrimp alkaline phosphatase (USB, Cleveland, Ohio, USA). After transformation of *E. coli* XL1-Blue (Bullock *et al.*, 1987) the resulting plasmid, designated pBlc1, was isolated and its composition was confirmed by restriction digest as well as double-stranded dideoxy sequencing (ABI PRISM 310 Genetic Analyzer; Applied Biosystems, Foster City, California, USA). On pBlc1, the recombinant protein was encoded in fusion with the amino-terminal type I signal peptide of OmpA and a C-terminal nine-residue *Strep*-tag II (Breustedt *et al.*, 2006; Schmidt & Skerra, 2007). The codon for the unpaired internal thiol residue Cys113 (numbering according to the mature full-length protein; Swiss-Prot entry P0A901) was subsequently replaced by a Ser codon *via* site-directed mutagenesis (Geisselsoder *et al.*, 1987) with the oligodeoxynucleotide 5′-GGT CCG GCC CGC TAA CCA GCG CAT G-3′, finally yielding pBlc2, which was used for recombinant protein production throughout this study.

2.2. Protein production and purification

Recombinant Blc was produced in *E. coli* K-12 strain JM83 (Yanisch-Perron *et al.*, 1985) harbouring pBlc2 by secretion as a soluble protein into the bacterial periplasm. Shake-flask cultures were grown in 2 l LB medium supplemented with 100 mg l^{-1} ampicillin at 295 K. Gene expression was induced at a cell density of OD_{550} = 0.5 by adding 0.2 mg l^{-1} anhydrotetracycline (Skerra, 1994). After further shaking for 3 h the cells were harvested by centrifugation, resuspended in 500 m*M* sucrose, 1 m*M* EDTA, 100 m*M* Tris–HCl pH 8.0 and kept on ice for 30 min. The resulting spheroplasts were sedimented by centrifugation and the supernatant containing the recombinant protein was recovered. The protein extract was dialyzed against 150 m*M* NaCl, 1 m*M* EDTA, 100 m*M* Tris–HCl pH 8.0 and applied onto a *Strep*-Tactin affinity column (Schmidt & Skerra, 2007) using the same buffer. The recombinant Blc was competitively eluted by the application of 2.5 m*M* D-desthiobiotin in the chromatography buffer. Elution

Table 1
Data-collection and refinement statistics for Blc.

Values in parentheses are for the highest resolution shell.

Data collection	
Space group	$I4_122$
Unit-cell parameters (Å)	$a = b = 88.94$, $c = 78.35$
Wavelength (Å)	1.5418
Resolution (Å)	30–2.6 (2.7–2.6)
Completeness (%)	98.7 (99.8)
Unique reflections	5024 (531)
Multiplicity	6.1 (6.2)
Mean $I/\sigma(I)$	34.7 (9.4)
$R_{\rm meas}$† (%)	4.5 (20.1)
Wilson B factor (Å^2)	36.4
Refinement	
Resolution (Å)	18.70–2.60 (2.67–2.60)
Reflections (working)	4787 (343)
Reflections (test)	236 (16)
$R_{\rm cryst}$‡ (%)	22.2 (30.6)
$R_{\rm free}$§ (%)	27.6 (46.0)
No. of protein atoms	1209
No. of water molecules	18
B values (Å^2)	
Protein atoms	36.0
Water molecules	32.0
Ramachandran plot (%)	
Favoured	93.2
Outliers	0.0
R.m.s.d. bonds (Å)	0.009
R.m.s.d. angles (°)	1.227

† $R_{\rm meas} = \sum_{hkl}[N/(N-1)]^{1/2}\sum_i |I_i(hkl) - \langle I(hkl)\rangle|/\sum_{hkl}\sum_i I_i(hkl)$. ‡ $R_{\rm cryst} = \sum_{hkl}||F_{\rm obs}| - |F_{\rm calc}||/\sum_{hkl}|F_{\rm obs}|$. § $R_{\rm free}$ is calculated as for $R_{\rm cryst}$, but with 5% of the reflections that were excluded from the refinement.

fractions were concentrated, applied onto a preparative Superdex 75 gel-filtration column (GE Healthcare, Uppsala, Sweden) using 150 m*M* NaCl, 1 m*M* EDTA, 100 m*M* Tris–HCl pH 8.0 as running buffer and eluted in a homogeneous peak. The yield was ∼1.5 mg purified protein per litre of *E. coli* culture.

2.3. Biochemical characterization

Analytical size-exclusion chromatography (SEC) was carried out on a Tricorn S75 column (Superdex 75 10/300 GL, bed volume $V_{\rm t}$ = 24 ml; GE Healthcare) at a flow rate of 0.5 ml min^{-1} using ÄKTApurifier instrumentation (GE Healthcare) with PBS (4 m*M* KH_2PO_4, 16 m*M* Na_2HPO_4, 115 m*M* NaCl) as the running buffer. Bovine serum albumin (66 kDa, $V_{\rm r}$ = 9.861 ml), carbonic anhydrase (29 kDa, $V_{\rm r}$ = 12.35 ml), myoglobin (17.05 kDa, $V_{\rm r}$ = 13.211 ml), cytochrome *c* (12.4 kDa, $V_{\rm r}$ = 14.11 ml) and aprotinin (6.5 kDa, $V_{\rm r}$ = 16.35 ml) were used as protein-size standards for calibration of the column, while the void volume was determined with blue dextran (V_0 = 8.08 ml).

Sedimentation-equilibrium experiments were performed using an XL-I analytical ultracentrifuge and a Ti-60 rotor equipped with a UV–Vis detector as well as an interference detector (Beckman, Fullerton, California, USA). An 0.8 mg ml^{-1} solution of purified recombinant Blc in 150 m*M* NaCl, 1 m*M* EDTA, 100 m*M* Tris–HCl pH 8.0 was applied to six-sector 12 mm path-length cells. The samples were centrifuged at 25 000 rev min^{-1} for 72 h at 277 K until equilibrium was reached, whereupon the protein gradient was measured by UV absorption at 280 nm. Data analysis was carried out with the *KaleidaGraph* software (Synergy Software, Reading, Pennsylvania, USA) as previously described (Zander *et al.*, 2007; Stromer *et al.*, 2004) using a value of 0.73 ml g^{-1} for the specific volume of the protein.

2.4. Crystallization and structure determination

Blc crystals were grown in hanging drops using the vapour-diffusion technique. Drops made up of 1 µl protein solution (10 mg ml^{-1}, dialyzed against 10 m*M* Tris–HCl pH 8.0) and 1 µl reservoir solution were equilibrated against 0.5 ml reservoir solution on siliconized glass cover slips. After about two months at 293 K, two crystals were obtained in the presence of 20%(*w*/*v*) PEG 10 000, 100 m*M* HEPES–NaOH pH 7.5. Blc crystals were harvested using nylon loops (Hampton Research, Laguna Niguel, California, USA), cryoprotected with Paratone N (Hampton Research), thereby removing excess mother liquor, and frozen in a 100 K nitrogen stream (Oxford Cryosystems, Oxford, England).

A native data set was collected on a MAR 345 imaging-plate detector (MAR Research, Hamburg, Germany) using monochromatic Cu $K\alpha$ radiation from a RU-300 rotating-anode generator (Rigaku, Tokyo, Japan) equipped with Confocal Max-Flux Optics (Osmic, Troy, Michigan, USA). Diffraction data were processed with the *XDS* package (Kabsch, 2010). The Blc crystals belonged to space group $I4_122$, with unit-cell parameters $a = b = 88.94$, $c = 78.35$ Å, containing one protein molecule per asymmetric unit (Table 1). The X-ray structure was solved by molecular replacement as implemented in *Phaser* (Storoni *et al.*, 2004) using the coordinates of a published Blc structure (PDB code 1qwd; Campanacci *et al.*, 2004) after deleting the N-terminal residues −17 to 4 as well as the loop residues 33–38 and 60–69 at the open end of the β-barrel. Model building was performed with *Coot* (Emsley & Cowtan, 2004), followed by restrained and TLS refinement using *REFMAC*5.5 (Murshudov *et al.*, 1997; Winn *et al.*, 2001). Finally, the structure was validated with *Coot* and *MolProbity* (Chen *et al.*, 2010).

Graphics were prepared with *PyMOL* (DeLano, 2002), while secondary-structure elements were assigned with *DSSP* (Kabsch & Sander, 1983). Superposition of structures was performed with *SUPERPOSE* (Krissinel & Henrick, 2004) and interfaces were analyzed with *PISA* (Krissinel & Henrick, 2007). The coordinates and structure factors for the refined Blc structure have been deposited in the RCSB Protein Data Bank (PDB code 3mbt).

3. Results and discussion

3.1. Recombinant expression and X-ray structure determination of Blc

Blc was secreted as a soluble protein into the periplasm of *E. coli* after its original type II signal peptide had been exchanged for the type I signal peptide of OmpA (Ghrayeb *et al.*, 1984), which has proven to be useful for recombinant protein export in many cases. In addition, the Cys residue at

position 1 of the mature polypeptide, which otherwise carries the lipid anchor of the natural lipoprotein, was replaced by Ala and the unpaired internal thiol residue Cys113 was substituted by Ser. Purification from the bacterial periplasmic extract was achieved *via* streptavidin affinity chromatography employing the *Strep*-tag II (Schmidt & Skerra, 2007), which was appended to the C-terminus. Blc was finally obtained as a homogeneous protein by preparative gel filtration.

During this purification step we noted that our recombinant Blc eluted as a fully monomeric protein. This was confirmed by analytical size-exclusion chromatography (SEC; Fig. 1), which revealed an apparent size of 13.0 kDa, which was even smaller than the calculated mass of 19.1 kDa for the mature protein and clearly indicated the absence of a dimer. Consequently, its oligomerization behaviour was further investigated by means of analytical ultracentrifugation (AUC), resulting in a monomeric molecular mass of 18.7 ± 0.4 kDa. This demonstrated that our recombinant Blc forms a stable monomer in solution, at least up to a concentration of about 40 µ*M*.

Crystallization of Blc was achieved at pH 7.5 with PEG 10 000 as precipitant. The obtained crystals belonged to space group $I4_122$ and contained one molecule per asymmetric unit. These crystals showed a lattice packing that differed from that of the previously described crystals of Blc-X in space group $P2_12_12_1$ with two molecules in the asymmetric unit. Interpretable main-chain electron density for Blc was observed for 149 of the 168 residues present in the construct. The missing residues comprised the N-terminal amino acids 1–8 and the C-terminal amino acids 158–168, *i.e.* the entire *Strep*-tag II.

3.2. Comparison of Blc crystallized in space group $I4_122$ with Blc-X in space group $P2_12_12_1$

The overall structure of the recombinant Blc analyzed here is very similar to that of Blc-X (PDB entries 1qwd and 2aco; Campanacci *et al.*, 2004, 2006), revealing the typical lipocalin fold characterized by a β-barrel with eight antiparallel strands (designated *A*–*H*) and a C-terminal α-helix (Fig. 2). In contrast, however, our structure clearly lacks the first two artificial β-strands (designated −1 and 1, respectively) outside the β-barrel that were previously described for Blc-X. This Blc variant carried 18 additional residues at the N-terminus (nine of which are visible in the crystallographic model; PDB entry 2aco) as well as four amino-acid replacements at the beginning of the mature sequence (Fig. 2*a*), both of which originate from the *att*B1 Gateway recombination sequence on the expression vector pDest17 (Campanacci *et al.*, 2006). Together with a stretch of the following native sequence, a two-stranded extra antiparallel β-sheet is formed in the crystal structure of Blc-X (Fig. 2*c*). The recombinant Blc prepared in the present study, however, lacks this extra peptide segment and has an almost native N-terminus, except for the missing lipid anchor at Cys1 (Fig. 2*a*).

Superposition of Blc with the two nonsymmetrical monomers *A* and *B* of the Blc-X crystal structure (PDB entry 2aco) resulted in r.m.s.d.s (over 149 C^{α} positions) of 0.68 and 0.89 Å, respectively, while mutual superposition of the latter two monomers yielded an r.m.s.d. of 1.07 Å. Apart from the artificial N-terminus in Blc-X, the largest conformational

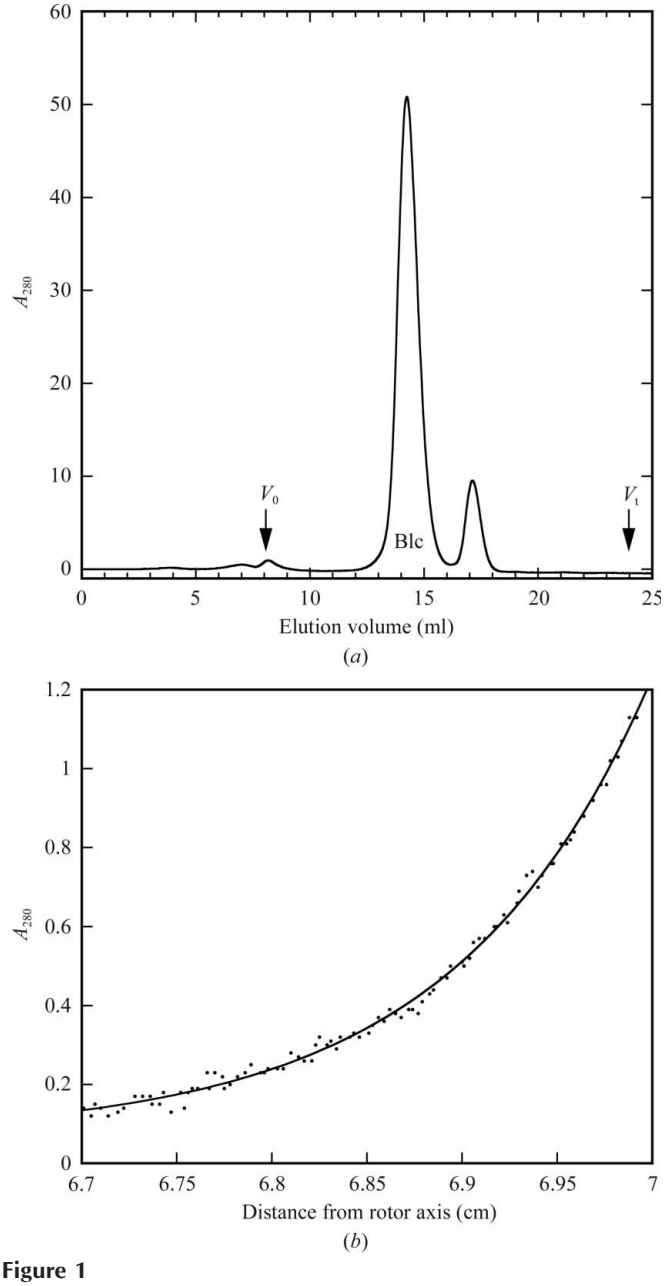

Figure 1
Biochemical analysis of the recombinant soluble Blc. (*a*) Analytical SEC of affinity-purified Blc, lacking its N-terminal lipid anchor and carrying a C-terminal *Strep*-tag II, on a Tricorn S75 column with PBS as running buffer. Blc elutes with a retention volume (V_r = 14.25 ml) corresponding to an apparent molecular size of 13.0 kDa. Essentially the same value was obtained when the chromatography was performed with 150 m*M* NaCl, 1 m*M* EDTA, 100 m*M* Tris–HCl pH 8.0 as running buffer (data not shown). The second small peak corresponds to nonproteinaceous contamination from the preceding affinity-chromatography step. (*b*) Analytical ultracentrifugation of Blc. The sample (protein concentration of 0.8 mg ml^{-1} in 150 m*M* NaCl, 1 m*M* EDTA, 100 m*M* Tris–HCl pH 8.0) was centrifuged at 25 000 rev min^{-1} until the concentration gradient, which was monitored *via* protein UV absorption at 280 nm, reached equilibrium. Curve fitting of the data (see §2.3) according to the one-species model led to a calculated mass of 18.7 ± 0.4 kDa.

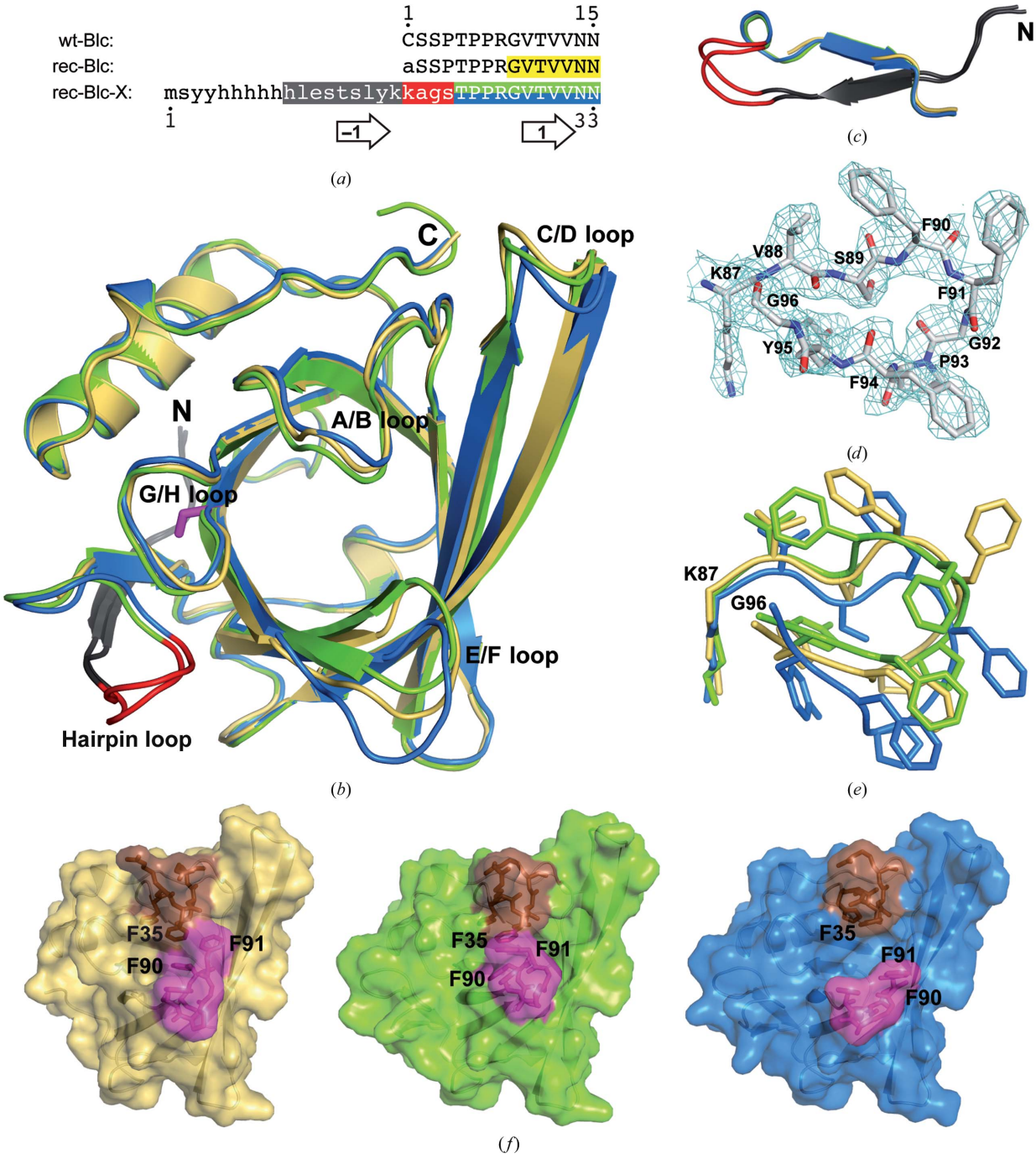

Figure 2
Comparison of Blc with Blc-X. (*a*) Amino-acid sequence alignment of the N-terminal region of wild-type *E. coli* Blc (wt-Blc), recombinant Blc from the present study (rec-Blc) and the previously reported Blc-X (rec-Blc-X) (Campanacci *et al.*, 2004, 2006). N-terminal sequence modifications are shown in lower case letters and residue numbering for the mature sequence of the wild type as well as recombinant Blc is shown above the alignment. The residues resolved in the corresponding crystal structures are highlighted: in yellow for rec-Blc as described here, starting from residue 9; for Blc-X, starting from residue 10, grey and red indicate artificial structural elements and green and blue the native sequence. β-Strands -1 and 1 of Blc-X are labelled with arrows below the sequence (using residue numbering as in the corresponding PDB entries 1qwd and 2aco). (*b*) Cartoon representation of rec-Blc (yellow) in space group $I4_122$ and of the two monomers *A* (green) and *B* (blue) from the previously published Blc-X structure in space group $P2_12_12_1$ (PDB entry 2aco) after superposition of the 149 C^{α} positions resolved for all structures. The largest structural deviations are found at the N-terminus (labelled 'N') and the *E*/*F* loop. The C113S mutation in rec-Blc is highlighted in magenta, while the C-terminal Pro residue preceding the *Strep*-tag II is labelled 'C'. (*c*) Close-up of the N-termini after superposition as above for Blc (yellow) and Blc-X monomers *A* (green) and *B* (blue). N-terminal extensions are depicted in grey and red as highlighted in the sequence alignment. (*d*) $2F_o - F_c$ map contoured at 1σ for the *E*/*F* loop of Blc (residues 87–96), illustrating the quality of the structural model. (*e*) Close-up of the *E*/*F* loop after superposition as above, including side chains. (*f*) Influence of the *A*/*B* and *E*/*F* loop conformations on the accessibility of the binding pocket in Blc. rec-Blc and monomers *A* and *B* of the Blc-X structure (PDB entry 2aco) are shown with yellow, green and blue surfaces, while the *A*/*B* and *E*/*F* loops are highlighted in brown and magenta, respectively. The Phe residues 35, 90 and 91 which restrict entry into the ligand cavity in the crystal structure of rec-Blc (left) are labelled.

differences were observed in the *E*/*F* loop, which was well ordered in our structure. This loop connects strands *E* and *F* of the β-barrel at its open end and adopts a distinct conformation in each of the three X-ray structures, apparently influenced by the differing crystal-packing environments (Figs. 2*d* and 2*e*). Further deviations occur at the loop regions connecting β-strands *A* to *B* and *C* to *D*, indicating increased flexibility, which has also been described for other members of this protein family, for example, human tear lipocalin (Breustedt *et al.*, 2009). The differing conformations of the *A*/*B* and *E*/*F* loops are critical for ligand binding as their arrangement restricts the accessibility of the deep ligand pocket. Only in monomer *B* of the Blc-X crystal structure do the *A*/*B* and *E*/*F* loops adopt a conformation that allows ligand binding. In our Blc structure and in monomer *A* of the Blc-X crystal structure the cavity is mostly shielded by the three Phe residues 35, 90 and 91 (Fig. 2*f*).

3.3. Reassessment of the proposed dimerization mechanism for Blc

Previous studies of Blc-X indicated a dimeric state both in the crystal lattice and in solution, suggesting the formation of an asymmetric functional homodimer with different affinities of its two subunits for lipid ligands (Campanacci *et al.*, 2004, 2006). In contrast, we observed Blc as a monomeric protein not only in the new crystal form but also in solution. To thoroughly compare the published Blc-X dimer interface with similar crystal-packing contacts in our Blc structure, we performed molecular-surface and interaction analyses using *PISA* (Krissinel & Henrick, 2007).

The dimer interface of Blc-X (PDB entry 2aco) is formed by 19 and 22 residues for molecules *A* and *B*, respectively, involving the N-terminal extra peptide segment together with the *E*/*F* loop and leading to 709 and 792 Å^2 buried surface area (BSA), respectively. These values are smaller than those of 786 and 825 Å^2 reported previously (Campanacci *et al.*, 2006), which may be attributed to the different, partly undisclosed, algorithms used. However, an even larger discrepancy was observed for the total solvent-accessible surface area (ASA) of the two Blc-X monomers. Using *PISA*, we calculated a total ASA of 8635 and 8784 Å^2 for molecules *A* and *B*, respectively, compared with the published value of 7800 Å^2 per monomer (Campanacci *et al.*, 2006). Similar larger values were obtained with the programs *DSSP* (Kabsch & Sander, 1983) and *AREAIMOL* (Collaborative Computational Project, Number 4, 1994).

Based on our calculations, an average of 8.6% of the total ASA of Blc-X becomes buried at the interface of the two monomers *A* and *B*. In contrast, in the new $I4_122$ crystals Blc forms its tightest contact with a symmetry-related monomer in a neighbouring unit *via* a different surface region around the N-terminus of strand *A* and the preceding loop that crosses the bottom of the β-barrel (not shown). This contact is accompanied by a significantly smaller BSA of 569 Å^2, which corresponds to merely 7.0% of the total ASA (8077 Å^2).

A striking feature of the previously described Blc-X dimer interface is the two-stranded antiparallel β-sheet that

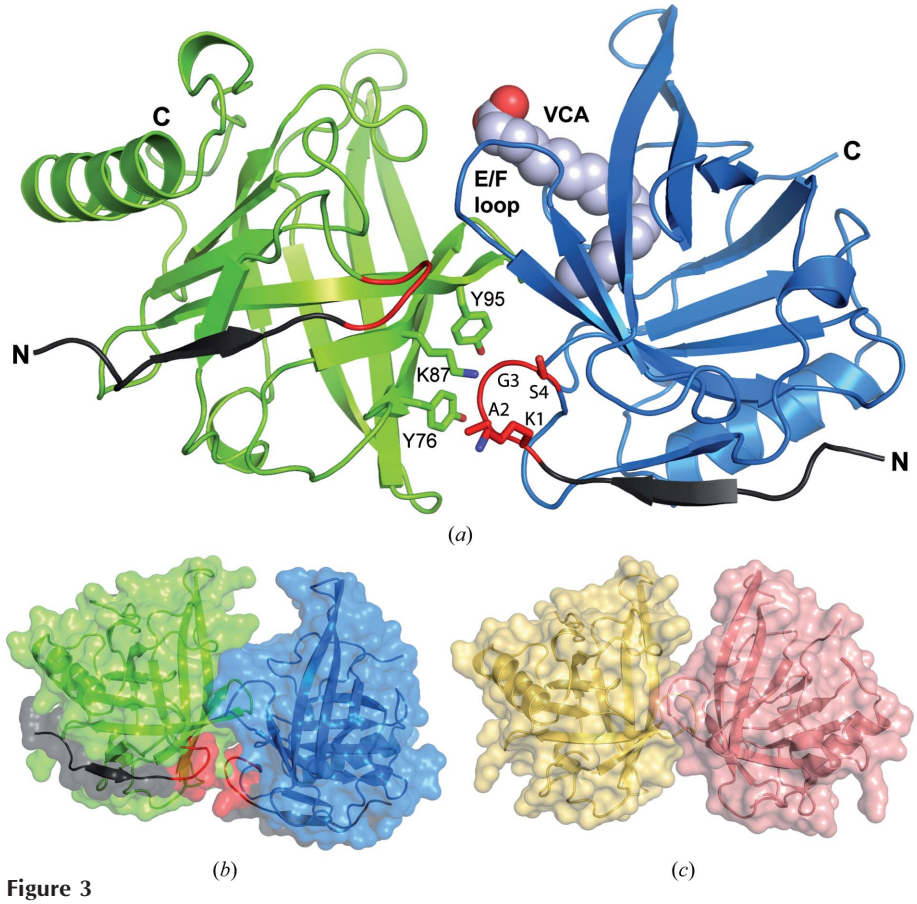

Figure 3
Comparison of the previously described Blc-X dimer with the crystal-packing environment of Blc. (*a*) The Blc-X dimer (chain *A*, green; chain *B*, blue) in the asymmetric unit of the $P2_12_12_1$ crystal structure (PDB entry 2aco) with vaccenic acid (grey spheres, O atoms red) occupying one ligand pocket. The N-terminal peptide extension of Blc-X, which forms β-strand −1 paired with strand 1 outside the β-barrel, is coloured grey for both monomers. The four mutated residues in the hairpin loop connecting the pair of β-strands (Lys-Ala-Gly-Ser), whose sequence positions correspond to the four N-terminal amino acids of mature wild-type Blc (*cf.* Fig. 2*a*), are coloured red (with N atom in blue). This segment of molecule *B* forms direct contacts with three side chains (Tyr94, Lys105 and Tyr113, corresponding to numbers 76, 87 and 95 of the native sequence, respectively) displayed on the β-barrel surface of molecule *A*. Next to this interaction, the *E*/*F* loops of both molecules form another tight almost symmetrical contact that involves several Phe side chains as noted previously (Campanacci *et al.*, 2006). (*b*) Surface representation of the proposed Blc-X dimer coloured as in (*a*). (*c*) Structurally equivalent crystal contact of Blc in space group $I4_122$ (yellow) with its symmetry mate (salmon) generated by a crystallographic twofold axis, which clearly illustrates the missing interface around the N-termini compared with the Blc-X dimer.

originates from the artificial 22 N-terminal residues. This small extra β-sheet itself neither interacts with the second monomer nor is it involved in interactions with symmetry-related neighbours. However, the hairpin loop that connects the two β-strands seems to be important for dimer formation of Blc-X (Figs. 3*a* and 3*b*): the loop of molecule *B* intimately interacts with molecule *A*, while the same loop of molecule *A* does not participate in an equivalent interaction, in line with the previously noted asymmetry of the dimer (Campanacci *et al.*, 2006). When all the artificially introduced N-terminal residues of molecule *B* were omitted from the surface analysis, the BSA was significantly reduced to 608 and 686 Å^2 for molecules *A* and *B*, respectively, *i.e.* 7.0 and 8.0% of the total ASA. These smaller values would hardly be significant for a true oligomeric state (Miller *et al.*, 1987). Moreover, the latter values are in a similar range to another crystal contact in the $P2_12_12_1$ space group with BSAs of 618 and 606 Å^2 for molecules *A* and *B*, respectively, corresponding to 7.2 and 7.0% of the ASA.

Taken together, two structural features are evident for Blc-X: (i) its N-terminal extension gives rise to an additional β-sheet, which conformationally fixes the loop in between, and (ii) substitution of the first four residues Cys-Ser-Ser-Pro of wild-type Blc by Lys-Ala-Gly-Ser within this loop (*cf.* Figs. 2*a* and 2*c*) leads to a unique intermolecular interaction (Fig. 3*a*), which possibly also stabilizes Blc-X dimer formation in solution. In contrast, the C-terminal *Strep*-tag II employed for affinity purification of Blc in our study is far away from the N-terminus (at least 35 Å distance) and is structurally disordered, thus clearly lacking defined interactions with neighbouring molecules in the $I4_122$ crystal lattice.

The dimer interface of Blc-X is further dominated by the interaction between the *E*/*F* loops of monomers *A* and *B*, which contribute 375 and 422 Å^2 BSA, respectively, corresponding to ∼53% of the total contact region including the N-terminal hairpin loop. Owing to the asymmetry of the dimer, the *E*/*F* loop adopts a distinct conformation in each monomer (Figs. 2*d* and 3*b*). Analysis of the alternative crystal packing of Blc in space group $I4_122$ revealed that a comparable but distinct contact occurs there with a symmetry mate related *via* a crystallographic twofold axis (Fig. 3*c*). This crystal contact shows a total BSA of 480 Å^2 and is again dominated by the *E*/*F* loop (residues 88–96), with a local BSA of 336 Å^2 on each molecule, corresponding to 70% of the total BSA in this region. Notably, in the present Blc structure the *E*/*F* loop shows a conformation different from both Blc-X monomers (Figs. 2*d* and 2*e*), suggesting structural flexibility. Therefore, dimerization *via* the *E*/*F* loop should be entropically disfavoured in solution. The fact that a crystal contact involving the *E*/*F* loop is observed in both crystal structures may be solely attributable to its largely hydrophobic nature.

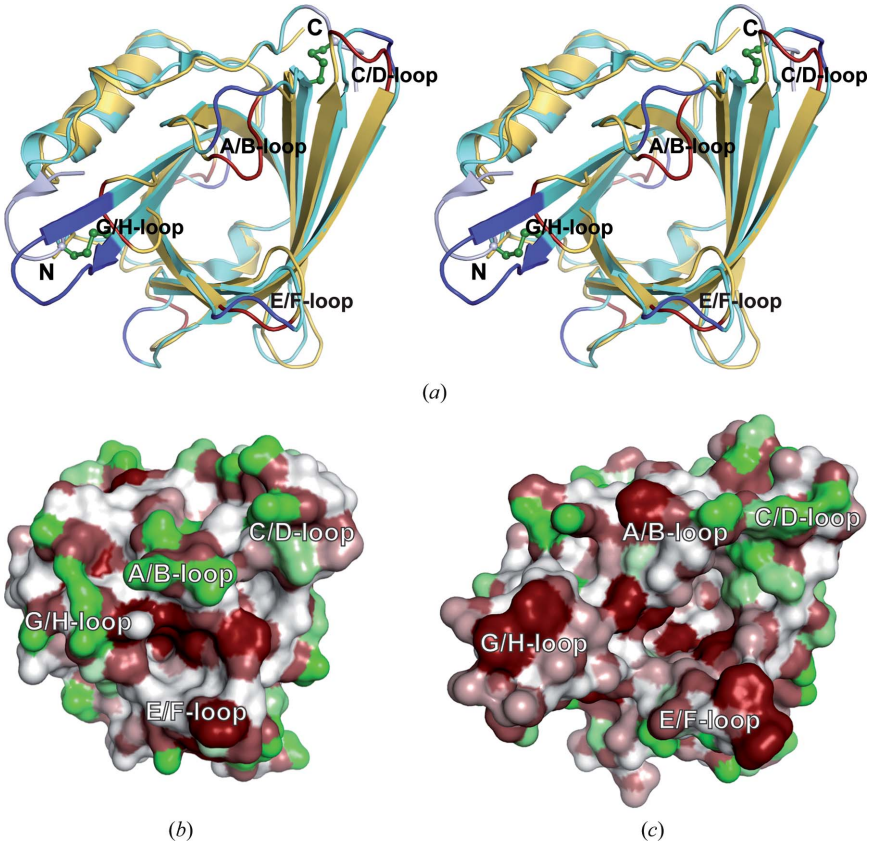

Figure 4
Structural comparison of Blc with human ApoD. (*a*) Superposition (in stereo) of Blc (yellow) and ApoD (cyan) using 139 equivalent C$^\alpha$ positions. Residues within the loop segments that do not match or show a deviation larger than 3 Å are highlighted in red and blue for Blc and ApoD, respectively. Additional residues at the N- and C-termini of ApoD are shown in grey. While Blc lacks disulfide bonds, the two disulfide bridges of ApoD that fix the N- and the C-terminus of the polypeptide chain to the β-barrel are depicted in ball-and-stick representation in green. (*b*) Representation of the surface hydrophobicity of Blc. Residues are coloured according to increasing hydrophobicity from green (hydrophilic) through white (neutral, including the polypeptide backbone) to brown (hydrophobic) using a group-wise parameter set (Tao *et al.*, 1999; Eichinger *et al.*, 2007). (*c*) The same orientation and surface representation for ApoD.

3.4. Biological implications

Although there has been considerable speculation about the biological function of Blc, its precise role in bacterial cell physiology is still unclear. This is partly owing to the circumstance that the *blc* gene is poorly transcribed and under the control of the σ factor RpoS, which directs expression in the stationary growth phase of *E. coli*. In fact, *blc* deletion strains grow normally under laboratory conditions. However, in the natural environment bacteria spend most of their life in the stationary phase and proteins synthesized under these conditions can be important for survival (Groat *et al.*, 1986; Bishop *et al.*, 1995).

Lipid trafficking between the inner and outer membranes of the Gram-negative bacterium is currently subject to intense interest. Yet, the mechanisms for the transperiplasmic movement of lipids are still largely unknown. In eukaryotes, lipid trafficking is usually mediated by lipid-transfer proteins or *via* vesiculation mechanisms. In Gram-negative bacteria vesiculation is less likely because of the structural barrier imposed by the peptidoglycan exoskeleton which separates the two membranes (Huijbregts *et al.*, 2000).

The biogenesis of bacterial lipoproteins, which are anchored on the periplasmic face of the outer membrane, depends on a specific transfer protein, suggesting that lipids themselves are transported by similar mechanisms (Tokuda & Matsuyama, 2004). Notably, several other members of the lipocalin family also constitute lipid-transfer proteins. For example, mammalian apolipoprotein D (ApoD) is the closest eukaryotic homologue of Blc and is also anchored in a lipid micelle, albeit *via* a different mechanism (Eichinger *et al.*, 2007). Structural comparison between Blc and ApoD results in 139 matching C^{α} positions out of 149 resolved residues in the Blc structure, with an overall r.m.s.d. as low as 1.37 Å (Fig. 4). Although Blc lacks both of the disulfide bonds present in ApoD, the characteristic lipocalin topology with the β-barrel and the attached α-helix is remarkably similar.

Differences between the two lipocalin structures are mainly observed in the strand-connecting loop regions at the open end of the β-barrel. The loops *A*/*B* and in particular *G*/*H* show the largest deviations. Loop *G*/*H* forms an extended hairpin structure in ApoD, resulting in a wider pocket that is ideally shaped for the accommodation of a steroid ligand. On the other hand, the *A*/*B* loop in Blc has a one-residue insertion compared with ApoD and partially shields the ligand pocket in the bacterial counterpart. In addition to variations in pocket size and accessibility, there are also differences in surface hydrophobicity. While ApoD shows distinct hydrophobic patches, which are likely to be involved in high-density lipoprotein (HDL) micelle association (Eichinger *et al.*, 2007), the hydrophobic surface areas of Blc are mainly confined to the interior of its cavity. This is in agreement with the presumed function of Blc in binding fatty acid-like ligands (Campanacci *et al.*, 2006), whereas membrane association should be mainly conferred by its N-terminal lipid anchor.

The physiological function of ApoD lies in the transport of the fatty acid arachidonate and also of steroids such as progesterone. Similarly, Blc might serve to capture ligands, possibly in a transient fashion, within the periplasmic space of *E. coli* as part of their transport and insertion into the bacterial cell envelope. In fact, this is supported by the earlier finding that Blc-X has a high affinity for lysophospholipids (LPLs), *i.e.* membrane intermediates of phospholipid metabolism (Campanacci *et al.*, 2006). Yet, in this regard mobility and freedom to reorient with respect to the outer membrane as well as flexibility of its binding site to accommodate and release lipid ligands in a dynamic fashion would be a clear advantage for Blc, which is much easier to achieve for a monomeric protein than for a structurally fixed dimer.

The authors wish to thank Ina Theobald and Susanne Berthold for technical assistance and Dr Klaus Richter for help with the analytical ultracentrifugation.

References

Bishop, R. E. (2000). *Biochim. Biophys. Acta*, **1482**, 73–83.
Bishop, R. E., Penfold, S. S., Frost, L. S., Holtje, J. V. & Weiner, J. H. (1995). *J. Biol. Chem.* **270**, 23097–23103.
Breustedt, D. A., Chatwell, L. & Skerra, A. (2009). *Acta Cryst.* D**65**, 1118–1125.
Breustedt, D. A., Schönfeld, D. L. & Skerra, A. (2006). *Biochim. Biophys. Acta*, **1764**, 161–173.
Bullock, W. O., Fernandez, J. M. & Short, J. M. (1987). *Biotechniques*, **5**, 376–379.
Campanacci, V., Bishop, R. E., Blangy, S., Tegoni, M. & Cambillau, C. (2006). *FEBS Lett.* **580**, 4877–4883.
Campanacci, V., Nurizzo, D., Spinelli, S., Valencia, C., Tegoni, M. & Cambillau, C. (2004). *FEBS Lett.* **562**, 183–188.
Chen, V. B., Arendall, W. B., Headd, J. J., Keedy, D. A., Immormino, R. M., Kapral, G. J., Murray, L. W., Richardson, J. S. & Richardson, D. C. (2010). *Acta Cryst.* D**66**, 12–21.
Collaborative Computational Project, Number 4 (1994). *Acta Cryst.* D**50**, 760–763.
DeLano, W. L. (2002). *PyMOL.* http://www.pymol.org.
Eichinger, A., Nasreen, A., Kim, H. J. & Skerra, A. (2007). *J. Biol. Chem.* **282**, 31068–31075.
Emsley, P. & Cowtan, K. (2004). *Acta Cryst.* D**60**, 2126–2132.
Flower, D. R. (1996). *Biochem. J.* **318**, 1–14.
Flower, D. R., North, A. C. & Sansom, C. E. (2000). *Biochim. Biophys. Acta*, **1482**, 9–24.
Geisselsoder, J., Witney, F. & Yuckenberg, P. (1987). *Biotechniques*, **5**, 786–790.
Ghrayeb, J., Kimura, H., Takahara, M., Hsiung, H., Masui, Y. & Inouye, M. (1984). *EMBO J.* **3**, 2437–2442.
Groat, R. G., Schultz, J. E., Zychlinsky, E., Bockman, A. & Matin, A. (1986). *J. Bacteriol.* **168**, 486–493.
Huijbregts, R. P., de Kroon, A. I. & de Kruijff, B. (2000). *Biochim. Biophys. Acta*, **1469**, 43–61.
Kabsch, W. (2010). *Acta Cryst.* D**66**, 125–132.
Kabsch, W. & Sander, C. (1983). *Biopolymers*, **22**, 2577–2637.
Kim, H. J., Eichinger, A. & Skerra, A. (2009). *J. Am. Chem. Soc.* **131**, 3565–3576.
Krissinel, E. & Henrick, K. (2004). *Acta Cryst.* D**60**, 2256–2268.
Krissinel, E. & Henrick, K. (2007). *J. Mol. Biol.* **372**, 774–797.
Miller, S., Lesk, A. M., Janin, J. & Chothia, C. (1987). *Nature (London)*, **328**, 834–836.
Murshudov, G. N., Vagin, A. A. & Dodson, E. J. (1997). *Acta Cryst.* D**53**, 240–255.
Schmidt, T. G. & Skerra, A. (2007). *Nature Protoc.* **2**, 1528–1535.
Skerra, A. (1992). *Nucleic Acids Res.* **20**, 3551–3554.
Skerra, A. (1994). *Gene*, **151**, 131–135.
Skerra, A. (2000). *Biochim. Biophys. Acta*, **1482**, 337–350.
Storoni, L. C., McCoy, A. J. & Read, R. J. (2004). *Acta Cryst.* D**60**, 432–438.
Stromer, T., Fischer, E., Richter, K., Haslbeck, M. & Buchner, J. (2004). *J. Biol. Chem.* **279**, 11222–11228.
Tao, P., Wang, R. X. & Lai, L. H. (1999). *J. Mol. Model.* **5**, 189–195.
Tokuda, H. & Matsuyama, S. (2004). *Biochim. Biophys. Acta*, **1693**, 5–13.
Winn, M. D., Isupov, M. N. & Murshudov, G. N. (2001). *Acta Cryst.* D**57**, 122–133.
Yanisch-Perron, C., Vieira, J. & Messing, J. (1985). *Gene*, **33**, 103–119.
Zander, H., Hettich, E., Greiff, K., Chatwell, L. & Skerra, A. (2007). *FEBS J.* **274**, 2603–2613.